Direct *ab initio* dynamics studies of proton transfer in hydrogen-bond systems

Robert L. Bell and Thanh N. Truong
Department of Chemistry, University of Utah, Salt Lake City, Utah 84112

(Received 10 August 1994, accepted 15 September 1994)

We present systematic direct *ab initio* dynamics studies of proton transfer in hydrogen-bond systems using the tautomerization in gas phase formamidine and its monohydrated complex as model reactions. The thermal rate constants were calculated using a canonical variational transition state theory (CVT) with multidimensional semiclassical tunneling corrections within a small-curvature ground-state approximation. The reaction valleys were calculated at the second-order Møller–Plesset (MP2) perturbation theory, Hartree–Fock (HF) and nonlocal Becke's half-and-half exchange and Lee–Yang–Parr correlation (BH&H–LYP) density functional theory (DFT) levels of theory using the 6-31 G(d,p) basis set. For accurate rate constants, the potential energy along the minimum energy path was scaled to match the single-point coupled cluster calculations including single and double excitations plus correction for triple excitation [CCSD(T)] at the MP2/6-31 G(d,p) classical barrier for each reaction. In the HF rate calculations, the HF frequencies were also scaled by a factor of 0.9. We found that adding a water to assist the proton transfer significantly enhances the tautomerization rate. Tunneling contributions in both systems are quite substantial and cannot be corrected by the Wigner approximation. We found that vibrational excitation of the solvent symmetriclike stretching mode would significantly enhance the rate of proton transfer in the formamidine–water complex. We also found that nonlocal DFT methods, particular the BH&H–LYP functionals studied here, can provide accurate potential energy information for dynamical calculations. Due to the computational advantage of DFT methods, prospects for dynamical studies of large polyatomic chemical reactions are quite encouraging. © *1994 American Institute of Physics.*

I. INTRODUCTION

Proton transfer is a common phenomenon in the chemical and biological sciences. In this study, we used proton transfers in formamidine and its monohydrated system as basic models for studying proton transfer processes in hydrogen bond systems for several reasons. First, formamidine and its amidine class have many biological and pharmaceutical importance.[1–5] Second, due to their size, numerous theoretical studies, including *ab initio* electronic structure[6–10] and semiclassical dynamical[11–13] calculations, have been reported, and thus can be compared to our study. Previous *ab initio* studies have provided information on the equilibrium, transition state structures, and barriers for tautomerization of gas phase formamidine and its monohydrated complex. Recently, we also reported comparisons between *ab initio* molecular orbital (MO) and density functional theory (DFT) methods for calculating structures, frequencies, and barrier heights for tautomerization in formamidine and its mono-, di-, and tri-hydrated complexes.[14] We found that nonlocal DFT, particularly with some mixing of Hartree–Fock exchange, can yield potential energy surface information at comparable accuracy to second-order Møller–Plesset perturbation theory (MP2) or better for some cases. Semiclassical dynamics calculations[11–13] had focused on the hydrated formamidine systems to investigate the roles of aqueous solvent in these processes.

Due to the size of the systems of interest, the conventional dynamical approach with the use of an analytical global potential energy function[15,16] (PEF) for reactive dynamics calculations would be too difficult. The main difficulty lies in the development of such PEF. In particular, the functional form of the PEF is based largely on the investigator's intuition *a priori* of what aspects of the potential energy surface are important to the dynamics. Fitting such functional forms to results of *ab initio* electronic structure calculations and experimental data is a very tedious and time consuming process which often yields little new knowledge. As the system size increases, this task becomes much more complex if not impossible. The additional complication is the number of *ab initio* energy points required for the fitting. It grows geometrically with the number of the internal geometrical parameters. For example, the formamidine–water complex used in this study has ten atoms. If one needs 10 points per internal coordinate degree of freedom, one would need a total of 10^{24} *ab initio* energy calculations! Direct dynamics methods provide an alternative approach for studying the dynamics of such systems. In the direct dynamics approach,[17–35] information needed for dynamical calculations can be calculated directly from electronic structure methods rather from an empirical analytical potential force field. Previous applications[6,23] of direct *ab initio* dynamics methods to study proton transfer reactions were limited to the Hartree–Fock method for calculating the reaction path.

Recently, we have significantly enhanced the applicability of the direct *ab initio* dynamics methods to large systems by introducing a focusing technique[34] and the use of computationally less demanding DFT methods.[35] The focusing technique also permits the use of more accurate *ab initio* methods in calculating the reaction valley. The direct *ab initio* dynamics methods used in this study are based on a full variational transition state theory with multidimensional

 0021-9606/94/101(12)/10442/10/$6.00

semiclassical tunneling corrections where the potential information can be calculated from a sufficiently accurate level of *ab initio* theory or density functional theory.

In this study, our objectives are to demonstrate the accuracy and applicability of our direct *ab initio* dynamics approach for studying quantal effects in proton transfer reactions and also to establish a reference point for our future studies of proton transfer reactions in biological systems. To do this, we have carried out rate calculations for the proton transfer in formamidine and the monohydrated complex using full variational transition state theory augmented with multidimensional semiclassical tunneling corrections. Particularly, we have investigated the quantum mechanical contributions namely tunneling and zero-point energy motions to the thermal rate constants as well as the effect of vibrational excitation on the reaction rate by examining the generalized frequencies and dynamical coupling constants as functions of the reaction coordinate. The reaction valleys were calculated at the MP2, HF, and nonlocal DFT levels of theory. Using the MP2 results as a reference point, we have tested the accuracy of two computationally less demanding approaches, namely, (i) the HF with scaling frequencies and energy, and (ii) the nonlocal DFT method.

This paper is organized as follows. Section II gives a brief outline of variational transition state theory and semiclassical multidimensional tunneling. Section III explains the computational details and Sec. IV gives the results and discussion.

II. THEORY

A. Variational transition state theory

Variational transition state theory has been described in detail elsewhere,[36–40] thus we only give a brief overview here. The canonical variational transition state rate constant (CVT) for a given temperature T is determined by minimizing the generalized transition state rate constant $k^{GT}(T,s)$ with respect to the location along the reaction coordinate s of the dividing surface which is orthogonal to the minimum energy path and intersects it at s. The reaction coordinate s is defined as the distance along the minimum energy path which is the steepest descent path in the mass-weighted internal coordinates along the Born–Oppenheimer potential from the saddle point to both the reactants and products with the origin at the saddle point and negative and positive values of s are towards the reactant and produce sides, respectively. Thus, the CVT rate constant is given by

$$k^{\mathrm{CVT}}(T)=\min_{s} k^{GT}(T,s), \tag{1}$$

where

$$k^{GT}(T,s)=\sigma \frac{k_B T}{h}\frac{Q^{GT}(T,s)}{Q^{R}(T)} e^{-V_{\mathrm{MEP}}(s)/k_B T}, \tag{2}$$

where σ is the reaction path multiplicity, k_B is Boltzmann's constant, h is Planck's constant and $V_{\mathrm{MEP}}(s)$ is the Born–Oppenheimer potential on the MEP, $Q^{GT}(T,s)$ is the partition function of the generalized transition state at s and $Q^{R}(T)$ is the reactant partition function. If by assuming that the electronic, rotational and vibrational degrees of freedom are separable, both $Q^{GT}(T,s)$ and $Q^{R}(T)$ can be written as products of the individual electronic, rotational and vibrational partition functions, Q_{elec}, Q_{rot}, and Q_{vib}, respectively. Since the rotational energy level spacings are small, we can replace the quantum rotational partition function by its classical counterpart without losing much accuracy. The vibrational partition functions were treated quantum mechanically within the harmonic approximation. The electronic partition functions for both the transition state and the reactant are assumed to cancel. Thus, the CVT rate constant is a hybrid rate constant where the reaction coordinate is treated classically while the remaining degrees of freedom are treated quantum mechanically.

Quantum effects along the reaction coordinate can be included by multiplying the CVT rate constant by the ground-state transmission coefficient to give the final rate constant as

$$k^{\mathrm{CVT/}G}(T)=\kappa^{\mathrm{CVT/}G}(T)k^{\mathrm{CVT}}(T). \tag{3}$$

B. Multidimensional semiclassical tunneling

Within the ground-state vibrationally adiabatic approximation, quantal effects for motion along the reaction coordinate is accounted for by the ground-state transmission coefficient[37,38,41–47] which is defined as the ratio of the thermally averaged quantal transmission probability, $P^{G}(E)$, to the thermally averaged classical transmission probability, $P^{G}_{C}(E)$,

$$\kappa^{\mathrm{CVT/}G}(T)=\frac{\int_0^\infty P^{G}(E)e^{-E/k_B T}\,dE}{\int_{V_a^G(s_*^{\mathrm{CVT}}(T))}^\infty e^{-E/k_B T}\,dE}, \tag{4}$$

where $s_*^{\mathrm{CVT}}(T)$ is the CVT dividing surface at temperature T, i.e., the location of s that minimizes the GTS rate constant in Eq. (2).

The $P^{G}(E)$ transmission probability at energy E is given by

$$P^{G}(E)=\frac{1}{(1+e^{2\theta(E)})}, \tag{5}$$

where $\theta(E)$ is the imaginary action integral. If the tunneling path is assumed to be along the MEP, i.e., the reaction path has zero curvature, $\theta(E)$ is given by

$$\theta(E)=\frac{2\pi}{h}\int_{s_<}^{s_>}\sqrt{2\mu(V_a^G(s)-E)}\,ds, \tag{6}$$

where $V_a^G(s)$ the vibrationally adiabatic ground-state potential defined by

$$V_a^G(s)=V_{\mathrm{MEP}}(s)+\epsilon_{\mathrm{int}}^G(s), \tag{7}$$

with $\epsilon_{\mathrm{int}}^G(s)$ denoting the zero-point energy of vibrational modes transverse to the MEP at s. $s_>$ and $s_<$ are the classical turning points defined by

$$V_a^G(s_<)=V_a^G(s_>)=E. \tag{8}$$

This is referred to as the zero-curvature tunneling (ZCT) method and the final rate constants are denoted as CVT/ZCT.

The effect of the reaction path curvature is included in the centrifugal-dominant small-curvature semiclassical adiabatic ground-state (CD-SCSAG) method[43] referred to as small-curvature tunneling (SCT). The CD-SCSAG approximation is a generalization of the Marcus–Coltrin approximation in which the tunneling path is distorted from the MEP out to the concave-side vibrational turning points in the direction of the internal centrifugal force. This results in a shorter tunneling path. In the SCT method, such a tunneling path, however, is not calculated explicitly but the curvature effects are accounted for in an effective reduced mass, $\mu_{\text{eff}}(s)$, which is used in calculating the barrier penetration integral [see Eq. (6)]. More detailed discussions on both ZCT and SCT methods can be found elsewhere.[37,38,41,43,44,46,48]

C. Dynamical coupling constants

To provide qualitative information on the effects of vibrational excitation on the proton transfer rate, we have also examined the dynamical B_{ks} coupling constants. The dynamical coupling constants describe how energy flows between the $3N$-7 vibrational modes and the reaction coordinate induced by the curvature of the reaction path.[49] If B_{ks} is large in the entrance channel then vibrational excitation of mode k will cause energy to flow into the reaction coordinate and enhance the reaction rate. The B_{ks} terms were calculated by Page and McIver's method.[50]

III. COMPUTATIONAL DETAILS

A. Electronic structure calculations

The minimum energy paths (MEP) for the tautomerization in gas phase formamidine and its monohydrated complex were calculated at both the MP2, HF, and nonlocal DFT levels using the second-order Gonzalez and Schlegel method[51] in mass-weighted internal coordinates with a step size of 0.1 amu$^{1/2}$ bohr for a total of 20 points in each direction. For nonlocal DFT, the combination of Becke's half-and-half (BH&H) method[52] for exchange and Lee–Yang–Parr (LYP) functional[53] for correlation was employed in calculating the reaction valley for tautomerization in the monohydrated formamidine system. Since the MEPs are symmetric for both systems considered here, only half of the MEP was actually needed. Hessian calculations were performed at selected points along the MEP according to the focusing technique. All calculations were done using the 6-31G(d,p) basis set. To test the accuracy of the reaction valley with respect to the step size, we have also calculated the MEP for the monohydrated system with a much smaller step size of 0.02 amu$^{1/2}$ bohr.

All electronic structure calculations were done using the G92/DFT program.[54]

B. Rate calculations

For dynamical calculations, a focusing technique was used to assure the convergence of the calculated rate constants with a minimal number of Hessian calculations required. This was done in two steps. First, a preliminary rate calculation with a coarse Hessian grid was carried out to estimate the regions containing the temperature dependent canonical transition state, $s_*^{\text{CVT}}(T)$, or having large curvature where the "corner cutting" effect would also be large. Finer grids were then calculated to improve the accuracy of the calculated canonical rate constants and small-curvature tunneling probabilities in these critical regions. This will be illustrated with more details below when we examine the convergence of the calculated rate constants with respect to the number of Hessian calculations. In all rate calculations, the potential energy along the MEP was scaled to yield the CCSD(T)//MP2 classical barriers.[14]

CVT and tunneling calculations were carried out using our new DiRate (Direct Rate) program.[55]

IV. RESULTS AND DISCUSSION

For clarity, we divide our discussion in two parts. In part A, we focus on the dynamics of tautomerization in formamidine and its monohydrated complex. For this discussion, the reaction valleys were calculated at the MP2/6-31G(d,p) level of theory with 41 Hessian points evenly distributed within the reaction coordinate range of [−2.0,2.0]. The step size of 0.1 amu$^{1/2}$ bohr was used to determine the MEPs. In part B, we illustrate the convergence of the focusing technique and discuss the accuracy of the HF and DFT methods for rate calculations.

A. Proton transfer in formamidine and its monohydrated complex

1. Reactants and transition states

In a separate report,[14] we discussed in detail the results from *ab initio* and density functional theory calculations on the tautomerization of gas phase formamidine and its mono-, di-, and trihydrated complexes. For the completeness of this report, we give a brief discussion on the electronic structure results for the gas phase and monohydrated cases and focus our attention on the dynamics. For the gas phase formamidine system as shown in Fig. 1, the C_2-symmetry transition state has the NCN angle compressed by 15 deg from its equilibrium value, i.e., from 121 to 106 deg at the MP2 level. The N–H bond was also stretched from 1.01 to 1.34 Å, a 33% increase in length. The inclusion of correlation energy at the MP2 or nonlocal DFT level only has a small effect in both the equilibrium or transition state structures for this system. The classical and zero-point energy corrected barrier heights are listed in Table I. The classical barrier height calculated at the CCSD(T)//MP2 level for this system is 48.8 kcal/mol. The zero-point correction calculated from the MP2 frequencies lowers this barrier by 3.6 kcal/mol.

For the proton transfer in the monohydrated system, the C_s-symmetry transition state at the MP2 level has the NCN bond angle compressed by only 3 deg as shown in Fig. 2. The N–H and O–H bonds were also stretched from 1.01 to 1.21 Å and from 0.98 to 1.30 Å, respectively. The effect of correlation at the MP2 and BH&H–LYP levels were found to significantly shorten the hydrogen bonds in both the equilibrium and transition state structures (see Fig. 2). The classical barrier height at the CCSD(T)//MP2 level is reduced by more than a factor of 2 from the gas phase value to 21.9

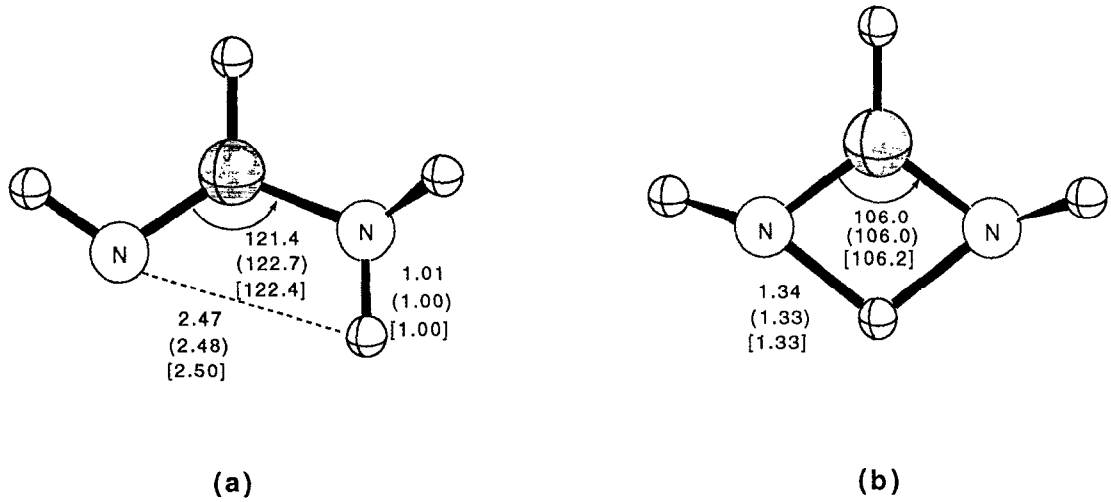

FIG. 1. Geometries of (a) the C_1-symmetry equilibrium structure and (b) the C_2-symmetry transition state structure for the tautomerization in the gas phase formamidine. Bond lengths are in Å and angles in degrees. Top numbers are the MP2 results. HF parameters are in parentheses and the BH&H-LYP results are in square brackets. The 6-31 G(d,p) basis set was used in all calculations.

kcal/mol. The zero-point energy correction at the MP2 level further lowers this barrier by another 4.1 kcal/mol (see Table I).

2. Reaction valleys

a. Gas phase formamidine. First, examination of the NCN angle and the active NH bond as functions of the reaction coordinate as shown in Fig. 3 elucidates the mechanism of the tautomerization in gas phase formamidine as a two-stage process in which changes in the structure along the reaction can be divided into two distinct parts, each involves different types of motions. Note this is different from a *two-step* process which involves a stable intermediate. More specifically, the NCN angle is first compressed from 121 to 106 deg while the active NH bond remains relatively constant until s reaches about -1.0 amu$^{1/2}$ bohr from the reactant. From the potential energy plot shown in Fig. 4, this step costs on the order of 20 kcal/mol. At this point, the NCN angle stays relatively constant while the hydrogen atom transfer from one N center to the other as its bond length is stretched from 1.01 to 1.34 Å as it reaches the saddle point. This step requires another 27 kcal/mol at the MP2 level. If it is the two-stage mechanism as indicated above, one would expect the active NH stretch frequency to remain relatively constant from the reactant to about $s=-1.0$ amu$^{1/2}$ bohr then start to drop steadily as it reaches the saddle point. This is in fact confirmed in the plot of the generalized frequencies as functions of the reaction coordinate as shown in Fig. 5.

b. Formamidine-water complex. The tautomerization in the formamidine–water complex involves a double proton transfer process which was found to proceed via a concerted two-stage mechanism. Again a two-stage process here means the structural changes along the MEP involve two distinct motions. More specifically, is shown in Fig. 6, the NCN angle is first compressed by 3 deg from the reactant to $s=-0.8$ amu$^{1/2}$ bohr while the active NH and OH bonds remain nearly constant about their equilibrium values. From the potential energy curves at the MP2 level shown in Fig. 7, this step requires about 10 kcal/mol of energy. Subsequently, the two hydrogen atoms from the two NH and OH active bonds synchronously transfer while the NCN angle remains nearly unchanged (see Fig. 6). The second stage costs about another 10 kcal/mol. The generalized frequencies plotted vs the reaction coordinate as shown in Fig. 8 further confirm this mechanism. Particular, the stretching frequencies of the two active NH and OH bonds slowly decrease by about 300 cm^{-1} from the reactant to the point on the MEP corresponding to an s value of about -0.8 amu$^{1/2}$ bohr. From this point, both frequencies drop rapidly by more than 1200 cm^{-1} when they reach the saddle point indicating both active NH and OH bonds are broken synchronously.

TABLE I. Calculated classical and zero-point corrected barriers (kcal/mol), $V^{\ddagger}$ and V_a^G, respectively, for formamidine and the formamidine–water complex.

Level	$\Delta V^{\ddagger}$	ΔV_a^G
Formamidine		
HF/6-31G(d,p)	61.0	57.0
MP2/6-31G(d,p)	47.0	43.4
MP4/6-31G(d,p)//MP2	48.0	44.4
CCSD(T)/6-31G(d,p)//MP2	48.8	45.2
BH&H-LYP/6-31G(d,p)	51.4	47.7
Formamidine–water complex		
HF/6-31G(d,p)	31.3	26.0
MP2/6-31G(d,p)	19.5	15.4
MP4/6-31G(d,p)//MP2	21.4	17.3
CCSD(T)/6-31G(d,p)//MP2	21.9	17.8
BH&H-LYP/6-31G(d,p)	20.7	16.6

3. Rate constants

Thermal rate constants calculated at different levels of dynamical theory are listed in Tables II and III, and the cor-

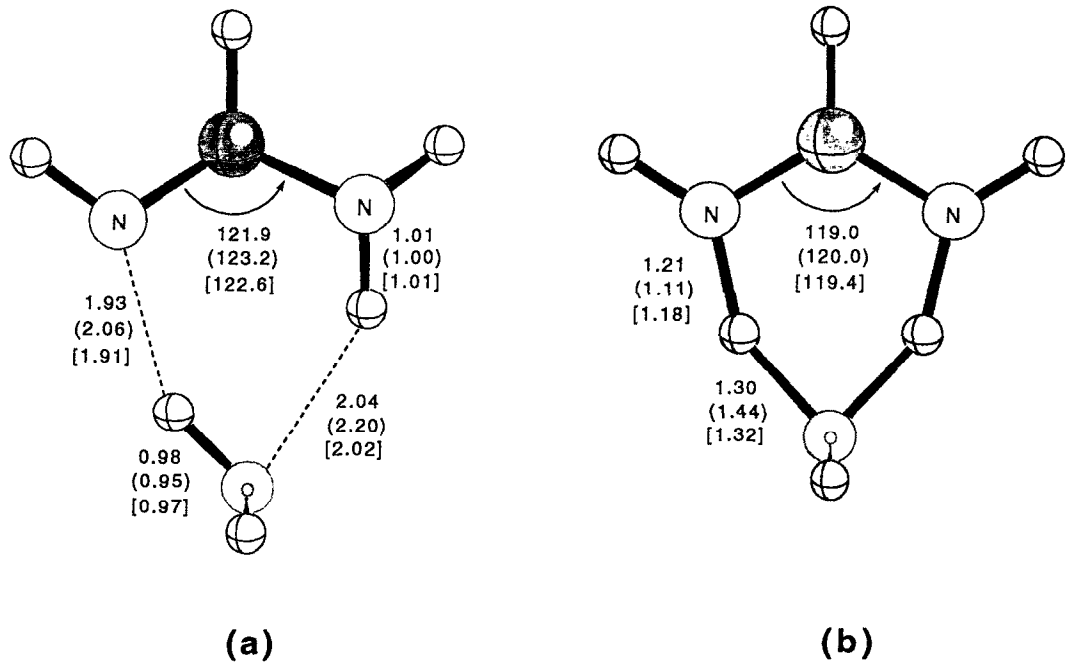

FIG. 2. Similar to Fig. 1, except for the tautomerization in the formamidine–water complex, (a) C_1-symmetry equilibrium and (b) C_s-symmetry transition state structure.

responding Arrhenius plots are shown in Figs. 9 and 10, respectively, for the tautomerization in gas phase formamidine and its monohydrated complex. In these rate calculations, the potential energy along the MP2–MEP was scaled by a factor of 1.038 and 1.123 to match the CCSD(T)//MP2 classical barrier heights for the tautomerization in gas phase formamidine and its monohydrated complex, respectively. Notice that the Arrhenius plots of CVT/SCT rate constants for both systems exhibit large curvatures indicating that tunneling plays a predominant role at low temperatures. In particular, at 200 K, tunneling enhances the tautomerization rate by 17 orders of magnitude for the gas phase system and by 5 orders of magnitude for the monohydrated complex. Even at 500 K, the SCT tunneling transmission coefficients are 7.9

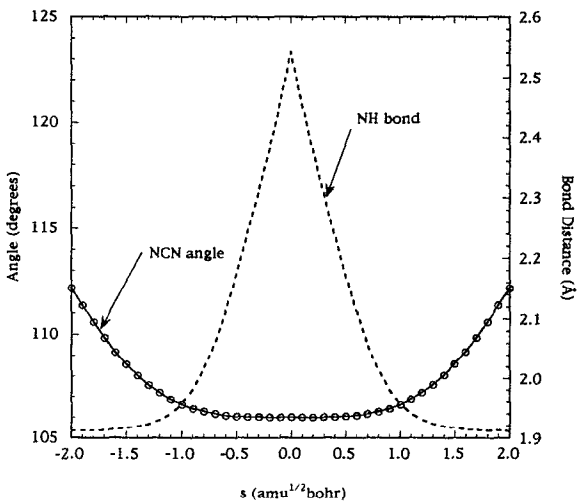

FIG. 3. Geometry along the minimum energy path plotted vs the reaction coordinate for the tautomerization in the gas phase formamidine, calculated at the MP2/6-31G(d,p) level. Solid line represents the NCN angle and the dashed line represents the active NH bond (NH bond that is being broken on the reactant side and is being formed on the product side). Circles indicate where structures are available.

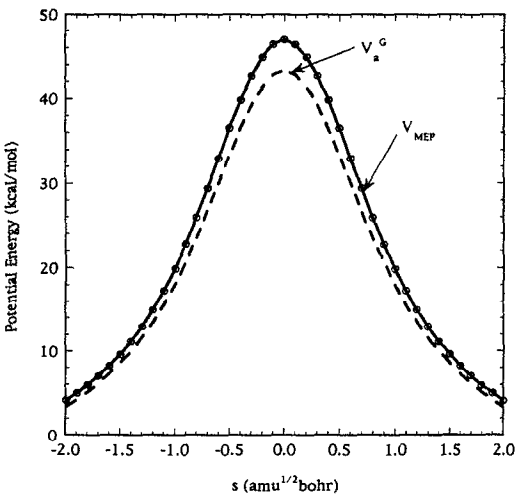

FIG. 4. Classical V_{MEP}(solid line) and zero-point corrected, V_a^G, (dashed line) potential energy along the MEP plotted vs the reaction coordinate for the tautomerization in the gas phase formamidine, calculated at the MP2/6-31G(d,p) level. Circles indicate where energies are available.

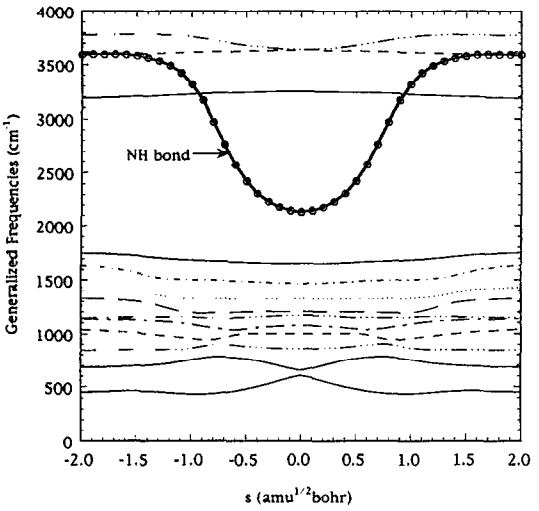

FIG. 5. Generalized frequencies plotted vs the reaction coordinate for the tautomerization in the gas phase formamidine, calculated at the MP2/6-31G(d,p) level. Darken solid line represents the frequency of the active NH stretching mode. Circles indicate where Hessians are available. Modes above 3000 cm^{-1} are of the NH and CH stretching vibrations. Modes below 1800 cm^{-1} are of bending vibrations.

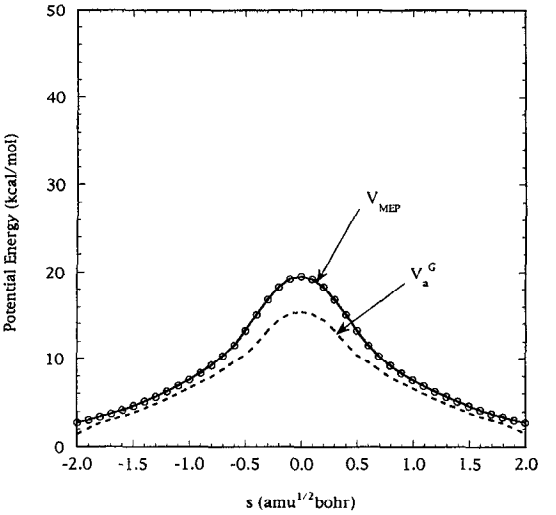

FIG. 7. Similar to Fig. 4, except for the tautomerization in the formamidine–water complex.

and 5.2, respectively. By comparing the TST/W and CVT/SCT results in Tables II and III, we found that Wigner corrections grossly underestimate the tunneling contributions in both systems. For instances, Wigner tunneling factors are less than 10 at 200 K for both systems with the errors of more than 16 and 4 orders of magnitude for the gas phase and formamidine–water complex, respectively. TST/ZCT-0 denotes TST rate constants with an Eckart tunneling corrections. Note that our Eckart tunneling model,[56] which does not require additional information other than at the stationary points as used by the TST/W method, significantly improves the estimation for the tunneling contributions. The errors are of one to two order of magnitude at 200 K and decrease as the temperature increases, i.e., when tunneling becomes less important (see Figs. 9 and 10). Comparing the CVT/ZCT and CVT/SCT results in Tables II and III and also shown in Figs. 9 and 10, we found that "corner cutting" on the multidimensional potential surface noticeably enhances the tunneling contribution for temperatures below 300 K for both systems, though by a slightly larger factor in the gas phase formamidine case. Our results are consistent with previous studies on similar systems.[23]

Placing a water molecule for direct assistance of the proton transfer as in the monohydrated formamidine complex

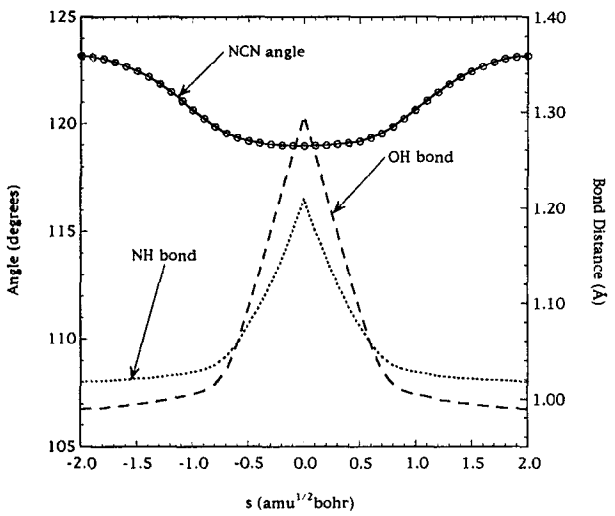

FIG. 6. Similar to Fig. 3, except for the tautomerization in the formamidine–water complex. Solid line is for the NCN angle, dotted line is for the active NH bond and dashed line is for the active OH bond.

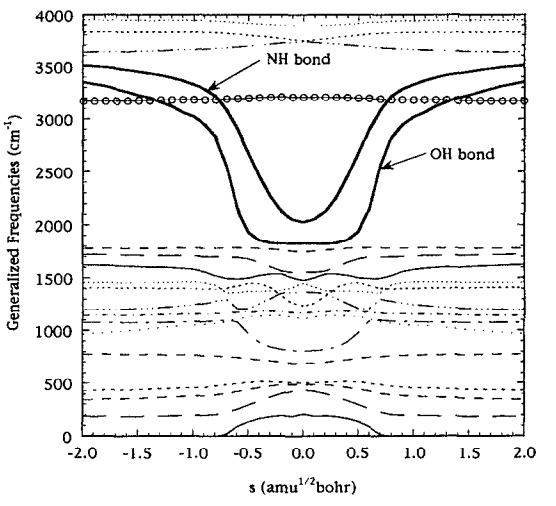

FIG. 8. Similar to Fig. 5, except for the tautomerization in the formamidine–water complex. Darken solid lines are for the active NH and OH stretching modes. Modes above 3000 cm^{-1} are of the NH, OH, and CH stretching vibrations. Modes between 500 and 1800 cm^{-1} are of bending vibrations. Modes below 500 cm^{-1} are of hydrogen bond vibrations.

TABLE II. Calculated thermal rate constants (s^{-1}) for the tautomerization in the gas-phase formamidine. The reaction valley was calculated at the MP2/6-31G(d,p) level of theory and the potential energy along the MEP was also scaled to match the CCSD(T) classical barrier.

T/K	TST	TST/W	TST/ZCT-0	CVT	CVT/ZCT	CVT/SCT
150	1.98E−51	3.13E−50	2.39E−23	1.98E−51	4.31E−23	6.82E−19
200	1.58E−35	1.47E−34	1.23E−20	1.58E−35	2.98E−20	9.55E−18
250	5.64E−26	3.56E−25	5.70E−18	5.64E−26	2.10E−17	7.52E−16
300	1.33E−19	6.25E−19	2.46E−15	1.33E−19	9.65E−15	8.37E−14
350	4.79E−15	1.78E−14	9.96E−13	4.79E−15	3.08E−12	9.75E−12
400	1.26E−11	3.87E−11	3.06E−10	1.26E−11	6.69E−10	1.11E−9
500	7.82E−7	1.82E−6	3.79E−6	7.82E−7	5.57E−6	6.19E−6
600	1.24E−3	2.39E−3	3.33E−3	1.24E−3	4.21E−3	4.39E−3
800	1.29E+1	1.96E+1	2.14E+1	1.29E+1	2.42E+1	2.45E+1
1000	3.40E+3	4.53E+3	4.66E+3	3.40E+3	5.02E+3	5.06E+3

enhances the tautomerization rate by more than 16 order of magnitude at room temperature (ratio of the two CVT/SCT rate constants). This factor includes contributions from the differences in the tunneling, zero point energy motion and classical barriers. To exclude the tunneling contribution, we examined the ratio of the CVT rate constants and found that adding a water as in the monohydrated system enhances the rate by more than 19 orders of magnitude at 300 K. Thus, tunneling lowers this enhancing factor. This is because the tunneling contribution in the monohydrated system is smaller due to the lower barrier than that of the gas phase system.

4. Effect of reagent vibration on the reaction rate

From the generalized frequency plot as shown in Fig. 8 for the monohydrated formamidine system, the large decreases in the stretching frequency for both the active NH and OH bonds at the saddle point, when compared to their corresponding reactant values, indicate that exciting these vibrational modes would greatly enhance the tautomerization rate. In particular, these frequencies drop by 1591 cm^{-1} for the amide NH stretching mode, and 1724 cm^{-1} for the H_2O "symmetric" stretching mode (this mode resembles the symmetric stretching mode in an isolated water molecule). This corresponds to a lowering of 4.55 or 4.93 kcal/mol in the vibrational adiabatic barrier if the active NH or the H_2O "symmetric" stretching mode is excited to its first excited state. The B_{ks} dynamical coupling constants as functions of the reaction coordinate for the active NH and OH stretching, and NCN bending modes as shown in Fig. 11 provide additional information on the effect of reagent vibration on the reaction rate. From the magnitudes of the B_{ks} values in the entrance channel we can predict that excitation of the H_2O "symmetric" stretching mode is much more efficient in enhancing the tautomerization rate than excitations of the active NH stretching or NCN bending mode. Such vibrationally excited-solvent-induced proton transfer phenomenon has not been observed experimentally, though it had also been found in a previous dynamical study[57] using a model potential energy function.

B. Accuracy of the direct *ab initio* dynamics methods

1. Convergence of the focusing technique

For this discussion, we used the tautomerization in the formamidine–water complex as a test case where the MEP was calculated at the MP2 level with the step size of 0.02 $amu^{1/2}$ bohr with the maximum of 28 Hessian points evenly distributed between s values of 0 and 1.2 $amu^{1/2}$ bohr. Due to the symmetry of the MEP, this is equivalent to a total of 59 Hessian points, including three stationary points, for the entire MEP. Using the CVT/SCT thermal rate constants calculated from these 28 calculated Hessian points as the reference point, we have calculated CVT/SCT rate constants with numbers of Hessian points less than the full 28, which were chosen by the focusing technique, and plotted in Fig. 12 with the percent difference in the rate constant at 300 K vs the number of Hessians used. We found that a minimum of 10 Hessian points is required for the convergence of the rate constant to within 10%. Furthermore, using a filtering tech-

TABLE III. Calculated thermal rate constants (s^{-1}) for the tautomerization in the formamidine–water complex. The reaction valley was calculated at the MP2/6-31G(d,p) level of theory and the potential energy along the MEP was also scaled to match the CCSD(T) classical barrier.

T/K	TST	TST/W	TST/ZCT-0	CVT	CVT/ZCT	CVT/SCT
150	4.29E−11	4.87E−10	3.44E−3	4.29E−11	5.02E−5	8.18E−2
200	1.77E−5	1.21E−4	1.25E−1	1.77E−5	3.36E−2	4.48
250	3.94E−2	1.86E−1	4.05	3.94E−2	3.36	1.07E+2
300	6.51	2.34E+1	9.93E+1	6.51	1.09E+2	1.30E+3
350	2.45E+2	7.13E+2	1.48E+3	2.46E+2	1.69E+3	1.02E+4
400	3.70E+3	9.09E+3	1.34E+4	3.70E+3	1.50E+4	5.71E+4
500	1.63E+5	3.14E+5	3.50E+5	1.63E+5	3.77E+5	8.52E+5
600	2.02E+6	3.33E+6	3.37E+6	2.02E+6	3.55E+6	6.14E+6
800	4.78E+7	6.52E+7	6.32E+7	4.78E+7	6.50E+7	8.81E+7
1000	3.28E+8	4.05E+8	3.91E+8	3.28E+8	3.99E+8	4.83E+8

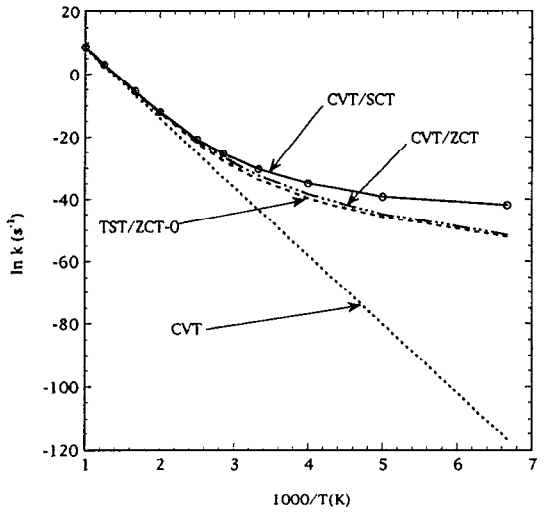

FIG. 9. Arrhenius plot of calculated CVT (dotted), TST/ZCT-0 (short dashed), CVT/ZCT (dashed–dotted) and CVT/SCT (solid) thermal rate constants vs 1000/T (K). The reaction valley was calculated at the MP2/6-31G(d,p) level of theory with the potential energy along the MEP further scaled by a factor to match the CCSD(T)//MP2/6-31G(d,p) classical barrier.

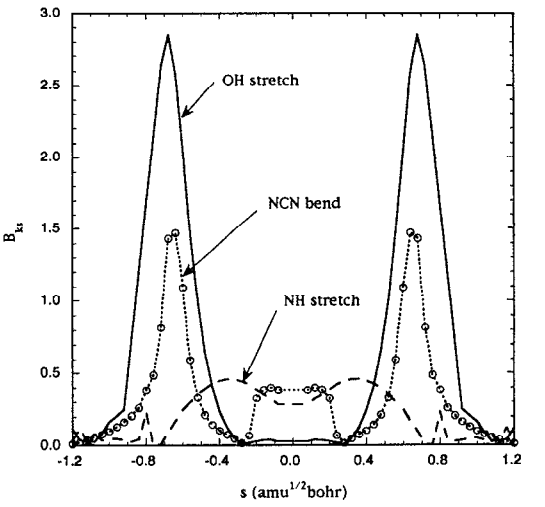

FIG. 11. Dynamical coupling constants plotted vs the reaction coordinate for selected vibrational modes for the tautomerization in the formamidine–water complex, calculated at the MP2/6-31G(d,p) level. Solid line is for the water "symmetric" stretch. The dotted and dashed lines are for the NCN bend and active NH stretch, respectively. Circles indicate where Hessians are available.

nique to remove noise in the calculated effective reduced mass slightly improves this convergence. Note even with 5 Hessian points, the calculated rate constant at 300 K converges to within a factor of 2 to the 28-point case. Though, for reactions with smaller tunneling contributions than in this case, a smaller number Hessians may be sufficient. In addition, not including the "corner cutting" effect from the bending modes, i.e., vibrational modes with frequency less than 1800 cm^{-1}, only introduces an error of less than 20%. In other words, this effect is larger in the stretching modes, particular for the active OH stretching mode (see Fig. 11).

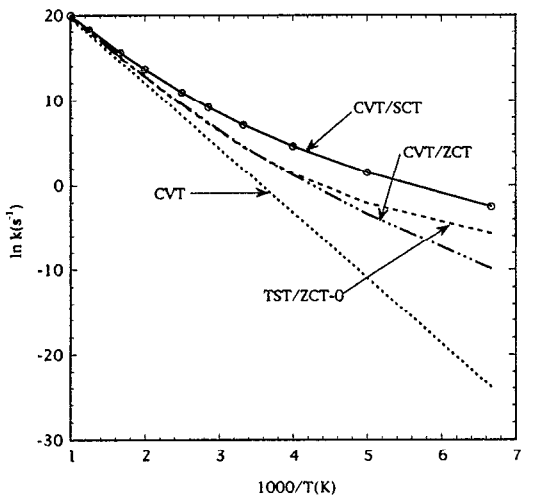

FIG. 10. Similar to Fig. 9, except for the tautomerization in the formamidine–water complex.

2. Direct dynamics with HF and DFT methods

Using the MP2 rate results for the tautomerization in the formamidine–water complex as a reference point, we have investigated the accuracy of two computationally less demanding approaches for calculating the potential energy information. One uses the HF theory, but in addition to scaling the classical barrier to the CCSD(T)//MP2 value, the HF frequencies were also scaled by a factor of 0.9. The other uses the nonlocal BH&H–LYP DFT method also with the same

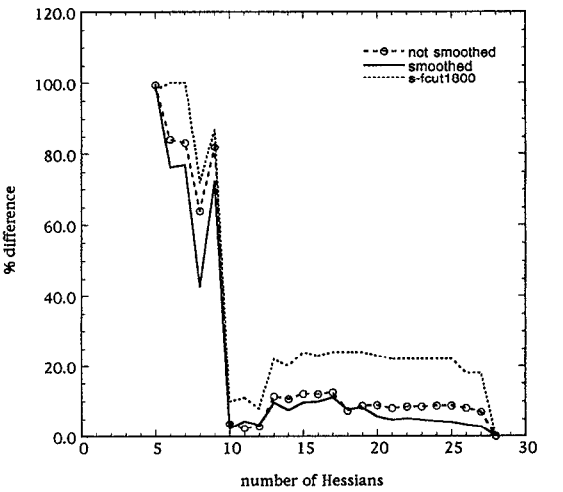

FIG. 12. Plot of the percent difference between the calculated thermal rate constants at 300 K (as functions of the number of Hessians chosen by the focusing technique) and the most accurate value calculated with 28 Hessians. Scaled MP2/6-31G(d,p) reaction valley was used. Solid line is for rate constants calculated with smoothed effective reduced mass and dashed line with no smoothing. Dotted line is with smoothing but with no "corner cutting" effects for modes below 1800 cm^{-1}.

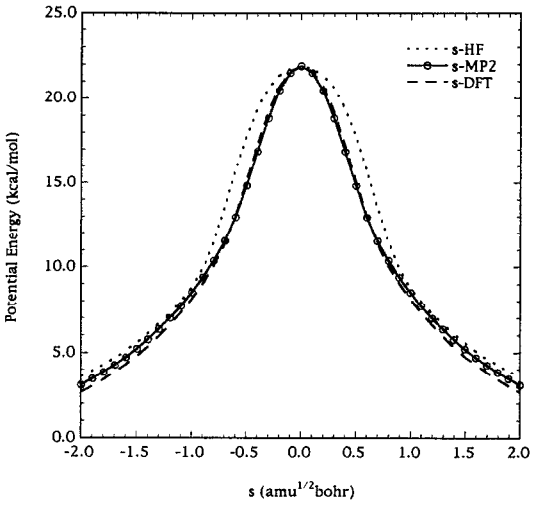

FIG. 13. Plot of the classical potential energy vs the reaction coordinate for the tautomerization of the formamidine–water complex. Solid line is for MP2, dashed line for BH&H–LYP and dotted line for HF. All potential curves were scaled to match the CCSD(T)/6-31G(d,p) classical barrier. Circles indicate where energies are available.

barrier scaling procedure. In both HF and DFT cases, the MEPs were calculated with the same step size of 0.1 amu$^{1/2}$ bohr as used in the MP2 calculations. The scaled MP2, HF, and DFT classical potential energy curves are plotted in Fig. 13. Notice that the MP2 and nonlocal DFT methods yield nearly identical results whereas the HF gives a noticeably wider potential width. One may expect the scaled HF approach would yield a smaller tunneling contribution. However, the transmission coefficients plotted vs $1/T$ in Fig. 14(b) indicate all three MP2, DFT, and HF methods yield nearly identical tunneling contributions. The small difference between the MP2 and HF tunneling contribution may result from the use of the unscaled-HF reaction path curvature in calculating the effective reduced mass. Since the HF method predicts much higher classical barrier, it would yield a larger reaction path curvature. As a consequence, it overestimates the "corner cutting" effect which can compensate for the wider potential width. Work is currently in progress to develop a more consistent scaling procedure for calculating the SCT tunneling contribution when the potential energy is scaled. The Arrhenius plot for the MP2, HF and DFT, CVT and CVT/SCT rate constants are also shown in Fig. 14. We found the HF-CVT rate constants are noticeably smaller than the MP2 and DFT rates. As results, the final HF CVT/SCT rate constants are also smaller. The excellent agreement between the MP2 and DFT rate constants further supports our earlier conclusion[35] on the use of nonlocal DFT methods for direct *ab initio* dynamics calculations.

Finally, it is interesting to point out that despite in theory, the computational demand for DFT calculations scales formally as N^3, in practice for the monohydrated system, we found that for a typical Hessian run with 90 basis functions, the MP2 calculation is faster by 15% in CPU time on a IBM RISC 370 workstation. This is due to (i) the MP2 procedure is computationally more efficient in the

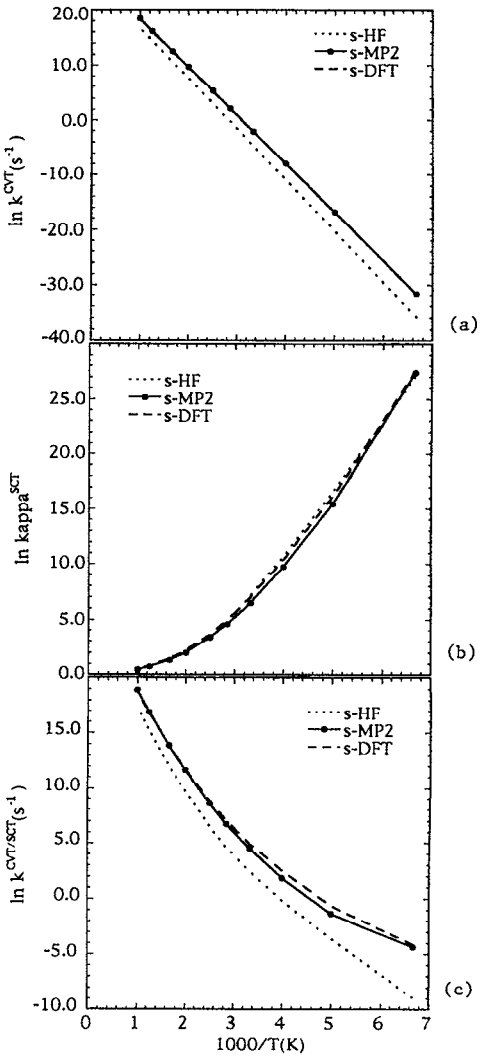

FIG. 14. Arrhenius plots of the individual contributions, (a) CVT rate, (b) k^{SCT}, and (c) the total CVT/SCT rate constants vs 1000/T (K). Dotted lines are results calculated from the HF reaction valley with scaled potential energy and frequencies; solid and dashed–dashed–dotted lines are results calculated from the scale MP2 and BH&H–LYP reaction valleys, respectively.

G92/DFT[54] program since it is a more established method, and (ii) mixing the HF exchange contribution as in the BH&H–LYP method increases the DFT computational demand. As the system size increases, the DFT method, however, will be more favorable not only in the CPU time but also in the disk storage requirement.

V. SUMMARY

We have carried out systematic direct *ab initio* dynamics studies of proton transfer in hydrogen bonding systems using the tautomerizations in gas phase formamidine and its monohydrated complex as prototypes. We found that the rate of proton transfer is greatly enhanced by adding a water to bridge the proton donor and acceptor sites. The double proton transfer process in the formamidine–water complex proceeds via a concerted two-stage mechanism. We also found

that the tunneling effect is significant. Even at 800 K, the tunneling contribution enhances the rate in both systems by nearly a factor of 2. The "corner cutting" effect on the multidimensional potential energy surface was found to further increase the tunneling probability. We found that the formamidine–water complex exhibits a vibrationally excited-solvent-induced proton transfer phenomenon, i.e., vibrational excitation of solvent stretching mode significantly enhances the proton transfer rate.

This study also provides tests on the applicability of direct *ab initio* dynamics methods. Particularly, we have tested the convergence of our earlier proposed focusing technique and the accuracy in dynamical results when the potential energy surface is calculated from a computationally less demanding method, such as the HF or DFT methods. We found that nonlocal DFT methods, particularly the BH&H–LYP functionals, can provide potential energy surface information for dynamical calculations at comparable accuracy with the MP2 level. Since the nonlocal DFT methods are computationally less demanding than correlated molecular orbital methods, prospects for direct *ab initio* dynamics studies of relatively large polyatomic reactions are now possible. The HF method also yields reasonably accurate rate constants. However, in this case, in addition to scaling the classical barrier to the more accurate results as used in both the MP2 and DFT calculations, the HF frequencies were also scaled by a factor of 0.9. Finally, with the use of the focusing technique, accurate rate constants for reactions with significant tunneling contributions such as those studied here can be obtained with 10 to 20 Hessian points along the MEP.

ACKNOWLEDGMENTS

This work was supported by the University of Utah and by the National Science Foundation through an NSF Young Investigator Award to T.N.T.

[1] S. A. Aziz and C. O. Knowles, Nature **242**, 418 (1973).
[2] R. W. Beeman and F. Matsumura, Nature **242**, 274 (1973).
[3] T. L. Johnson and C. O. Knowles, Gen. Pharmacol. **14**, 591 (1983).
[4] M. Kaneda, Y. Oomura, O. Ishibashi, and N. Akaike, Neurosci. Lett. **88**, 253 (1988).
[5] R. J. Grant, in *The Chemistry of Amidates and Imidates*, edited by S. Patai (Wiley, New York, 1975), Chap. 6.
[6] A. D. Isaacson, L. Wang, and S. Scheiner, J. Phys. Chem. **97**, 1765 (1993).
[7] K. A. Nguyen, M. S. Gordon, and D. G. Truhlar, J. Am. Chem. Soc. **113**, 1596 (1991).
[8] R. A. Poirier, D. Majlessi, and T. J. Zielinski, J. Comp. Chem. **7**, 464 (1986).
[9] T. Yamabe, K. Yamashita, M. Kaminoyama, M. Koizumi, A. Tachibana, and K. Fukui, J. Phys. Chem. **88**, 1459 (1984).
[10] K. Yamashita, M. Kaminoyama, T. Yamabe, and K. Fukui, Theor. Chim. Acta **60**, 303 (1981).
[11] M. Nagaoka, Y. Okuno, and T. Yamabe, J. Am. Chem. Soc. **113**, 769 (1991).
[12] M. Nagaoka, Y. Okuno, T. Yamabe, and K. Fukui, Can. J. Chem. **70**, 377 (1992).
[13] M. Nagaoka, Y. Okuno, and T. Yamabe, J. Chem. Phys. **97**, 8413 (1992).
[14] Q. Zhangm, R. L. Bell, and T. N. Truong, J. Phys. Chem. (in press).
[15] G. C. Schatz, Rev. Mod. Phys. **61**, 669 (1989).
[16] D. G. Truhlar, M. S. Gordon, and R. Steckler, Chem. Rev. **87**, 217 (1987).
[17] K. K. Baldridge, M. S. Gordon, D. G. Truhlar, and R. Steckler, J. Phys. Chem. **93**, 5107 (1989).
[18] B. Calef and A. Redondo, Chem. Phys. Lett. **223**, 1 (1994).
[19] R. Car and M. Parrinello, in *Simple Molecular Systems at Very High Density*, edited by A. Polian, P. Loubeyre, and N. Boccara (Plenum, New York, 1989), p. 455.
[20] S. M. Colwell and N. C. Handy, J. Chem. Phys. **82**, 1281 (1985).
[21] C. J. Doubleday, J. W. J. McIver, and M. Page, J. Phys. Chem. **92**, 4367 (1988).
[22] M. J. Field, Chem. Phys. Lett. **172**, 83 (1990).
[23] B. C. Garrett and C. F. Melius, in *Theoretical and Computational Models for Organic Chemistry*, edited by S. J. Formosinho, I. G. Csizmadia, and L. G. Arnaut (Kluwer, Dordrecht, 1991), pp. 25–54.
[24] A. Gonzalez-Lafont, T. N. Truong, and D. G. Truhlar, J. Chem. Phys. **95**, 8875 (1991).
[25] A. Gonzalez-Lafont, T. N. Truong, and D. G. Truhlar, J. Phys. Chem. **95**, 4618 (1991).
[26] S. K. Gray, W. H. Miller, Y. Yamagychi, and H. F. Schaefer, J. Am. Chem. Soc. **103**, 1900 (1981).
[27] B. Hartke and E. A. Carter, J. Chem. Phys. **97**, 6569 (1992).
[28] T. Helgaker, E. Uggerud, and H. J. A. Jensen, Chem. Phys. Lett. **173**, 145 (1990).
[29] D. Malcome-Lawes, J. Am. Chem. Soc. Faraday Trans. 2 **71**, 1183 (1975).
[30] D. K. Remler and P. A. Madden, Mol. Phys. **70**, 921 (1990).
[31] A. Tachibana, H. Fueno, and T. Yamabe, J. Am. Chem. Soc. **108**, 4346 (1986).
[32] D. G. Truhlar and M. S. Gordon, Science **249**, 491 (1990).
[33] I. Wang and M. J. Karplus, J. Am. Chem. Soc. **95**, 8160 (1973).
[34] T. N. Truong, J. Chem. Phys. **100**, 8014 (1994); T. N. Truong and T. J. Evans, J. Phys. Chem. **98**, 9558 (1994).
[35] T. N. Truong and W. T. Duncan, J. Chem. Phys. (in press).
[36] D. G. Truhlar and B. C. Garrett, Accounts Chem. Res. **13**, 440 (1980).
[37] D. G. Truhlar, A. D. Isaacson, and B. C. Garrett, in *Theory of Chemical Reaction Dynamics*, edited by M. Baer (CRC, Boca Raton, FL, 1985), Vol. 4, pp. 65–137.
[38] S. C. Tucker and D. G. Truhlar, in *New Theoretical Concepts for Understanding Organic Reactions*, edited by J. Bertran and I. G. Csizmadia (Kluwer, Dordrecht, Netherlands, 1989), pp. 291–346.
[39] W. L. Hase, Accounts Chem. Res. **16**, 258 (1983).
[40] J. C. Keck, Adv. Chem. Phys. **13**, 85 (1967).
[41] D. G. Truhlar, A. D. Isaacson, R. T. Skodje, and B. C. Garrett, J. Phys. Chem. **86**, 2252 (1982).
[42] D. G. Truhlar and B. C. Garrett, Annu. Rev. Phys. Chem. **35**, 159 (1984).
[43] D.-h. Lu, T. N. Truong, V. S. Melissas, G. C. Lynch, Y. P. Liu, B. C. Garrett, R. Steckler, A. D. Isaacson, S. N. Rai, G. C. Hancock, J. G. Lauderdale, T. Joseph, and D. G. Truhlar, Comput. Phys. Comm. **71**, 235 (1992).
[44] Y.-P. Liu, D.-h. Lu, A. Gonzalez-Lafont, D. G. Truhlar, and B. C. Garrett, J. Am. Chem. Soc. **115**, 7806 (1993).
[45] B. C. Garrett, T. Joseph, T. N. Truong, and D. G. Truhlar, Chem. Phys. **136**, 271 (1989).
[46] B. C. Garrett, N. Abushalbi, D. J. Kouri, and D. G. Truhlar, J. Chem. Phys. **83**, 2252 (1985).
[47] A. D. Isaacson, B. C. Garrett, G. C. Hancock, S. N. Rai, M. J. Redmon, R. Steckler, and D. G. Truhlar, Computer Phys. Comm. **47**, 91 (1987).
[48] B. C. Garrett and D. G. Truhlar, J. Phys. Chem. **95**, 374 (1991).
[49] W. H. Miller, N. C. Handy, and J. E. Adams, J. Chem. Phys. **72**, 99 (1980).
[50] M. Page and J. W. McIver, Jr., J. Chem. Phys. **88**, 922 (1988).
[51] C. Gonzalez and H. B. Schlegel, J. Phys. Chem. **94**, 5523 (1990).
[52] A. D. Becke, J. Chem. Phys. **98**, 1372 (1993).
[53] C. Lee, W. Yang, and R. G. Parr, Phys. Rev. B **37**, 785 (1988).
[54] M. J. Frisch, G. W. Trucks, H. B. Schlegel, P. M. W. Gill, B. G. Johnson, M. W. Wong, J. B. Foresman, M. A. Robb, M. Head-Gordon, E. S. Replogle, R. Gomperts, J. L. Andres, K. Raghavachari, J. S. Binkley, C. Gonzalez, R. L. Martin, D. J. Fox, D. J. Defrees, J. Baker, J. J. P. Stewart and J. A. Pople, GAUSSIAN 92/DFT (Gaussian, Inc., Pittsburgh, 1993).
[55] T. N. Truong, *DiRate (unpublished)* (University of Utah, Salt Lake City, 1993).
[56] T. N. Truong, and D. G. Truhlar, J. Chem. Phys. **93**, 1761 (1990).
[57] D. Borgis, G. Tarjus, and H. Azzouz, J. Phys. Chem. **96**, 3188 (1992).